

Biochemical and Mutational Studies of the *Bacillus cereus* CECT 5050T Formamidase Support the Existence of a C-E-E-K Tetrad in Several Members of the Nitrilase Superfamily^{V†}

Pablo Soriano-Maldonado,¹ Ana Isabel Martínez-Gómez,¹ Montserrat Andújar-Sánchez,¹ José L. Neira,^{2,3} Josefa María Clemente-Jiménez,¹ Francisco Javier Las Heras-Vázquez,¹ Felipe Rodríguez-Vico,¹ and Sergio Martínez-Rodríguez^{1*}

Departamento de Química Física, Bioquímica y Química Inorgánica, Universidad de Almería, 04120 Almería, Spain¹; Instituto de Biología Molecular y Celular, Universidad Miguel Hernández, 03202 Elche, Alicante, Spain²; and Complex Systems Physics Institute, 50009 Zaragoza, Spain³

Received 12 February 2011/Accepted 10 June 2011

Formamidases (EC 3.5.1.49) are poorly characterized proteins. In spite of this scarce knowledge, ammonia has been described as playing a central role in the pathogenesis of human pathogens such as *Helicobacter pylori*, for which formamidase has been shown to participate in the nitrogen metabolic pathway. Sequence analysis has revealed that at least two different groups of formamidases are classified as EC 3.5.1.49: on the one hand, the derivatives of the FmdA-AmdA superfamily, which are the best studied to date, and on the other hand, the derivatives of *Helicobacter pylori* AmiF. Here we present the cloning, purification, and characterization of a recombinant formamidase from *Bacillus cereus* CECT 5050T (BceAmiF), the second member of the AmiF subfamily to be characterized, showing new features of the enzyme further supporting its relationship with aliphatic amidases. We also present homology modeling-based mutational studies confirming the importance of the Glu140 and Tyr191 residues in the enzymatic activities of the AmiF family. Moreover, we can conclude that a second glutamate residue is critical in several members of the nitrilase superfamily, meaning that what has consistently been identified as a C-E-K triad is in fact a C-E-E-K tetrad.

Formamidases (formamide amidohydrolases; EC 3.5.1.49) catalyze the hydrolysis of the amide bond of formamide, producing ammonia and formic acid. These enzymes were proposed to be a different group of amidases as a result of studies of the ability of different microorganisms to use short aliphatic amides as a nitrogen or carbon source by virtue of producing different amidases which hydrolyze amides to ammonia and the corresponding organic acid (18, 24). Formamidases have been detected in the following organisms: *Helicobacter pylori* (48), *Methylophilus methylotrophus* (53, 54), *Paracoccidioides brasiliensis* (5, 6), *Aspergillus (Emericella) nidulans* (17, 24), and *Alcaligenes (Ralstonia) eutrophus* (18). However, the classification of these enzymes has not proven easy, as there are other similar amidases which present activity toward formamide, such as the acetamidase from *Mycobacterium smegmatis* (13, 34) and different aliphatic amidases (14, 16, 35).

Most of the studies concerning the natural function of formamidases are related to the human pathogen *H. pylori* (9, 10, 48, 50, 51), for which ammonia has been proved to play a central role in human pathogenesis (51). This is in part due to the resistance of this compound to the acid shocks produced in the stomach (see reference 51 and references therein). Al-

though urea seems to be the main source of ammonia in the gastric environment, in times of urea shortage this bacterium has been proposed to produce this compound through alternative pathways, such as via amino acid deaminases and amidases (see reference 50 and references therein). Among these amidases, formamidase (AmiF) and aliphatic amidase (AmiE; EC 3.5.1.4) were shown to be different enzymes due to the ability of an AmiE-defective mutant of *H. pylori* to retain the ability to hydrolyze formamide (47). The same group then proved that the primary structures of AmiE and AmiF are intimately related, suggesting a possible evolution of formamidases from aliphatic amidases after ancestral gene duplication (48). This hypothesis was further supported by the elucidation of the crystal structure of *H. pylori* AmiF, which revealed that this enzyme belongs to the nitrilase superfamily and maintains unaltered the characteristic C-E-K triad of the family (23). Furthermore, the relationship between AmiF and AmiE is also supported by the concomitant monocistronic, acid-induced transcription of both genes (43). AmiF- and AmiE-mediated ammonia production by *H. pylori* may not be sufficient for its acid resistance, but it might act as a starting point for the urea cycle of this bacterium, suggesting the importance of these enzymes when urea availability is low (see reference 51 and references therein). On the other hand, the same authors also proposed that due to the important role of ammonia in nitrogen metabolism, ammonia production by both AmiF and AmiE might allow the production of sufficient intracellular concentrations of ammonia without alkalization of the cellular environment (51). However, the first hypothesis (absence of urea) seems more reliable, based on studies carried out on

* Corresponding author. Mailing address: Departamento de Química Física, Bioquímica y Química Inorgánica, Universidad de Almería, Edificio CITE I, Carretera de Sacramento s/n, 04120 La Canáda de San Urbano, Almería, Spain. Phone: 34 950 015850. Fax: 34 950 015615. E-mail: srodrig@ual.es.

† Supplemental material for this article may be found at <http://aem.asm.org/>.

the complex acid adaptation system showing the expression/regulation and acid dependence of *H. pylori* AmiF and AmiE (32, 39, 43, 50–52).

Despite the vast amount of information on *H. pylori* formamidase regulation and involvement in acid adaptation, the biochemical and structural properties of these enzymes have scarcely been described. The present study reports the cloning, purification, and characterization of a recombinant formamidase from *Bacillus cereus* CECT 5050T (BceAmiF). Based on a homology-based model, we specifically altered three amino acids of BceAmiF, i.e., Trp136, Glu140, and Tyr191, to investigate their biochemical roles in catalysis. Together with sequence analysis and kinetic and binding studies, information on the importance of these residues in recognition and hydrolysis of the substrates for several members of the nitrilase superfamily is discussed in this work.

MATERIALS AND METHODS

Materials. All chemicals were analytical grade and were used without further purification. Talon metal-affinity resin was purchased from Clontech Laboratories, Inc. The different amides and acids, hydroxylamine, and acetohydroxamic acid used in this work were from Sigma and Panreac.

Microbes and culture conditions. *Bacillus cereus* CECT 5050T was used as a possible donor of the formamidase gene (encoding BceAmiF). It was grown at 30°C for 24 h on Luria-Bertani (LB) agar plates (1% tryptone, 0.5% yeast extract, 0.5% NaCl, pH 7.2, 1.5% agar). *Escherichia coli* DH50' was used to clone the BceAmiF gene, and *E. coli* BL21(DE3) was used to overexpress it.

Cloning and sequence analysis of BceAmiF. A single-colony isolate of *Bacillus cereus* CECT 5050T was chosen for DNA extraction, using a slightly modified version of the method described by van Eys et al. (37, 49). A sample of the supernatant containing genomic DNA (about 5 µl) was used to amplify the gene encoding the formamidase by PCR. The primers used were designed based on the sequence under GenBank accession number AE016877 (BC_3939 gene [denoted as an amidase gene]). These were BceAmiF5 (5'-CATATGGGGTAGTA GTGGAAGTATGGTAAAG-3') and BceAmiF3 (5'-CTCGAGGGGATCCAC GCGGAACCAAGAATGAATCGTTTTTTTTTA-3') and included NdeI and XhoI restriction sites, respectively. The latter also included a thrombin recognition site (underlined in the BceAmiF3 sequence). The PCR fragment obtained was purified from agarose gel by use of a QIAquick kit (Qiagen) and was subcloned using a StrataClone PCR cloning kit (Stratagene). The isolated subcloning plasmid was purified using a QIAprep Spin miniprep kit (Qiagen) and then digested using NdeI and XhoI. The digested fragment was purified from agarose gel by use of a QIAquick kit (Qiagen) and then ligated into pET22b+ plasmid (Novagen) cut with the same enzymes to create plasmid pTCM16. The resulting construct allows the production of recombinant BceAmiF fused at the C terminus to a polyhistidine tag (His₆ tag), allowing its removal by thrombin treatment.

Once the fragment had been cloned, it was sequenced at least twice by using standard T3 and T7 primers, using the dideoxy nucleotide dye sequencing method in an ABI 377 DNA sequencer (Applied Biosystems). The sequence was aligned and compared with all relevant available amino acid sequences by using the Basic Local Alignment Search Tool (BLAST) (1). The Clustal W XXL program (28) was used to compare sequences and to calculate similarity percentages. Phylogenetic studies were carried out using the TREEVIEW program (42).

Expression of the BceAmiF gene. The *E. coli* BL21(DE3) strain containing pTCM16 was grown in LB medium supplemented with 100 µg ml⁻¹ of ampicillin. A single colony was transferred into 10 ml of LB medium with ampicillin at the above-mentioned concentration in a 100-ml flask. This culture was incubated overnight at 37°C with shaking. Five hundred milliliters of LB with the appropriate concentration of ampicillin was inoculated with 5 ml of the overnight culture in a 2-liter flask. After 2 h of incubation at 37°C with vigorous shaking, the optical density at 600 nm (OD₆₀₀) of the resulting culture was 0.3 to 0.5. For induction of expression of the BceAmiF gene, isopropyl-β-D-thiogalactopyranoside (IPTG) was added to a final concentration of 0.2 mM, and the culture was continued at 34°C for a further 6 h. The cells were collected by centrifugation (Beckman JA2-21 centrifuge; 7,000 X g, 277 K, 10 min) and stored at -20°C until use.

Purification of BceAmiF. *E. coli* BL21(DE3)/pTCM16 cells were resuspended in 30 ml wash buffer (300 mM NaCl, 0.02% NaN₃, 50 mM sodium phosphate, pH 7.0). The cell walls were disrupted on ice by sonication using a UP200S ultrasonic processor (Hielscher GmbH, Germany) for 6 periods of 30 s each with pulse mode 0.5 and a sonic power of 60%. The pellet was precipitated by centrifugation (Beckman JA2-21 centrifuge; 10,000 X g, 4°C, 20 min) and discarded. The supernatant was applied to a column packed with Talon metal-affinity resin (Clontech Laboratories, Inc.) and then washed three or four times with wash buffer. After being washed, the BceAmiF enzyme was eluted with elution buffer (100 mM NaCl, 0.02% NaN₃, 50 mM imidazole, 2 mM Tris, pH 8.0). Protein purity was determined at different stages of the purification by SDS-PAGE. An additional gel filtration chromatography step was carried out using a Superdex 200 gel filtration column (GE Healthcare) in a BioLogic DuoFlow fast-performance liquid chromatography (FPLC) system (Bio-Rad) to eliminate any DNA coeluting with the protein. The purified enzyme was concentrated using an Amicon ultrafiltration system with Amicon YM-3 membranes and then dialyzed against 100 mM sodium citrate, pH 6.0, and stored at 4°C. Protein concentrations were determined from the absorbance, based on the extinction coefficient ($\epsilon = 77,810 \text{ M}^{-1} \text{ cm}^{-1}$) of tyrosine residues (20). Protein without the His₆ tag was obtained using a thrombin cleavage capture kit from Novagen (Germany). This protein was used as a control to ascertain the importance of the His₆ tag in the enzymatic activity of BceAmiF.

Mutation of BceAmiF Trp136, Glu140, and Tyr191 and purification of the resulting mutants. Mutagenesis was performed using a QuikChange II site-directed mutagenesis kit (Agilent, Barcelona, Spain) following the manufacturer's protocol, using the plasmid pTCM16 as the template. Mutations were confirmed by using the dideoxy nucleotide dye sequencing method in an ABI 377 DNA sequencer (Applied Biosystems). The plasmids containing the mutations (pSER80 [E140D], pSER81 [W136H], and pSER82 [Y191F]) were transformed into *E. coli* BL21(DE3), and their overexpression and purification were carried out as described above for the wild-type enzyme.

Molecular mass analysis. Size-exclusion chromatography-high-performance liquid chromatography (SEC-HPLC) analysis was performed to calculate the molecular mass of the wild-type enzyme, using a nondenatured protein molecular weight marker kit (Sigma-Aldrich Quimica S.A., Madrid, Spain). A biocompatible HPLC system (Finnigan SpectraSystem HPLC; Thermo, Madrid, Spain) equipped with a BioSep-SEC-S2000 column (Phenomenex, Barcelona, Spain) was equilibrated and eluted with 100 mM buffers from pH 5.5 to 9.0 at a flow rate of 0.5 ml min⁻¹. Absorbance was monitored at 280 nm. The molecular size of the monomeric form was estimated by SDS-PAGE, using a low-molecular-weight marker kit (GE Healthcare, Barcelona, Spain). Matrix-assisted laser desorption/ionization-tandem time of flight (MALDI-TOF-TOF) peptide mass fingerprinting was carried out to ascertain the nature of the purified protein on an LTQ Velos instrument with a Proxeon Easy-nLC system (Thermo, Madrid, Spain). The measured tryptic peptide masses were searched through the NCBI nr database, using Mascot software (Matrix Science, London, United Kingdom).

Enzyme assay and protein characterization. Standard enzymatic reactions were carried out with BceAmiF (2 µg/ml; 52 nM), together with formamide (100 mM) as a substrate, in 100 mM sodium citrate buffer (pH 6.0) in 520-µl reaction mixtures. Each reaction mixture was incubated at 50°C for 15 min, and the reaction was stopped by retrieving an aliquot of 75 µl followed by addition of 675 µl of 1% H₃PO₄. After centrifugation, the supernatant was analyzed by HPLC. An HPLC system (Finnigan SpectraSystem HPLC system; Thermo) equipped with a Luna 5-µm C₁₈ (2) column (4.6 X 250 mm; Phenomenex) was used to detect formamide and formic acid. The mobile phase was 95% 20 mM KH₂PO₄, pH 2.5, and 5% methanol, pumped at a flow rate of 0.4 ml min⁻¹ and measured at 210 nm. The same method was used to determine the optimum temperature and pH. The temperature range was 20 to 70°C, and the buffers used were 100 mM sodium citrate (pH 4.0 to 6.0), 100 mM sodium cacodylate (pH 6.0 to 7.5), 100 mM phosphate buffer (pH 6.0 to 8.0), and 100 mM borate-HCl or NaOH (pH 8.0 to 9.0). Thermal stability of the enzyme was determined after a 30-min preincubation at different temperatures from 20 to 80°C in 100 mM sodium citrate buffer, pH 6.0, followed by the standard activity assay. To analyze the effects of different compounds (NaCl, KCl, MgCl₂, CaCl₂, PbCl₂, HgCl₂, EDTA, dithiothreitol [DTT], and iodoacetamide) on enzyme activity, samples of BceAmiF (52 nM) were incubated with the compounds in 100 mM sodium citrate buffer, pH 6.0 (final volume, 20 µl), at 4°C for 60 min, followed by the standard enzyme assay. BceAmiF mutant activities were measured with formamide, using the standard activity assay described above.

Substrate specificity of the enzyme was tested with different aliphatic amides and amino acid amides, such as formamide, acetamide, propionamide, butyramide, isobutyramide, glycinamide, alaninamide, leucinamide, and urea. Kinetic studies of the enzyme were conducted using formamide as the substrate. Car-

bonyltransferase activities were assayed using the different aliphatic amides mentioned above and their corresponding acids as donors, with hydroxylamine as the acceptor.

CD experiments. The secondary structures of the E140D and Y191F mutants were compared with that of wild-type BceAmiF by using far-UV circular dichroism (CD) spectra recorded with a Jasco J810 CD spectrometer (Jasco Inc., Madrid, Spain) equipped with a Jasco PTC-423S/15 Peltier accessory. The protein concentration was 1.5 μM in 1 mM sodium citrate buffer, pH 6.0. CD measurements were taken at 25°C using a 1-mm-path-length cuvette. Spectra were acquired from 250 to 190 nm at a scan rate of 50 nm min⁻¹, with a response time of 2 s and a bandwidth of 1 nm. For each protein, a baseline scan (buffer) was subtracted from the average of six scans to give the final averaged scan.

For thermal denaturation experiments, CD spectra were measured in 1 mM sodium citrate buffer at pH 6.0 at a protein concentration of 5 μM in a 1-mm cuvette. Thermal denaturation measurements were monitored by measuring the changes in 0^h-helices at 222 nm. Denaturation data were collected at a scan rate of 0.2°C min⁻¹, with a response time of 8 s and a bandwidth of 1 nm, and the temperature was increased from 25°C to 95°C.

The thermal transitions of wild-type and mutated BceAmiF were analyzed using a two-state model. The spectral parameters were fitted directly to the following equation by nonlinear least-square analysis:

$$S_{\text{obs}} = \frac{S_N + S_U \exp\left[-\frac{\Delta H_{\text{VH}}}{R} \left(\frac{1}{T} - \frac{1}{T_m}\right)\right]}{1 + \exp\left[-\frac{\Delta H_{\text{VH}}}{R} \left(\frac{1}{T} - \frac{1}{T_m}\right)\right]}$$

where S_{obs} is the ellipticity at 222 nm and S_N ($A_N + B_N T$) and S_U ($A_U + B_U T$) refer to the linear dependence of the native (N) and unfolded (U) states, which have the slopes B_N and B_U , respectively. ΔH_{VH} is the apparent change in van't Hoff enthalpy, R is the universal gas constant, T is the temperature in Kelvin, and T_m is the melting temperature or the transition midpoint at which 50% of the protein is unfolded. Fitting of the data was carried out with Kaleidagraph (Abelbeck software).

Fluorescence studies. Fluorescence emission spectra were measured at 25°C using an FP-6500 spectrofluorimeter (Jasco Inc.) equipped with an ETC 273T Peltier accessory for wild-type BceAmiF and the E140D and Y191F mutants. All measurements were carried out with protein concentrations in the range of 0.79 to 0.95 μM in a 10-mm cuvette. Enzymes were excited at 280 nm in order to obtain the intrinsic fluorescence spectra. The binding of formamide and phosphate to the enzymes was monitored using the decrease of fluorescence emission at 340 nm. Excitation and emission bandwidths were 3 and 10 nm, respectively. Fluorescence measurements were corrected for dilution.

The saturation fraction, Y , can be expressed as follows:

$$Y = \frac{K[\text{ligand}]}{1 + K[\text{ligand}]}$$

where K is the characteristic microscopic association constant and $[\text{ligand}]$ is the free concentration of phosphate or formamide. This concentration can be expressed by the equation $[\text{ligand}] = [\text{ligand}]_{\text{T}} - nY[\text{enzyme}]$, where $[\text{ligand}]_{\text{T}}$ is the total concentration of ligand, n is the number of active sites, and $[\text{enzyme}]$ is the concentration of enzyme. Moreover, the saturation fraction, Y , can be calculated as follows:

$$Y = \frac{\Delta F_{\text{corr}}}{\Delta F_{\text{max}}} = \frac{F(\text{ligand}) - F(0)}{F(00) - F(0)}$$

where $F(0)$, $F(\text{ligand})$, and $F(00)$ are the corrected fluorescence intensities for the protein solutions without ligand, at a concentration of ligand equal to that of formamide or phosphate, and at a saturating ligand concentration, respectively. Fitting of the data was carried out with Origin (OriginLab, Northampton, MA).

Modeling studies. The model of BceAmiF was obtained by the Swiss-Model server (46), using the structure of the formamidase from *Helicobacter pylori* (HpyAmiF) (77% similarity; Protein Data Bank [PDB] accession no. 2DYU), solved at 1.75 Å (23). The stereochemical geometry of the final model was validated by the QMean server and the PROCHECK program (4, 30, 31).

Manual model building and distance measurements of the structures were performed with Swiss PDB Viewer (21, 25) and PyMol (<http://www.pymol.org/>).

Accession numbers. The nucleotide and protein sequences of the formamidase gene of *B. cereus* CECT 5050T have been deposited in the GenBank database

RESULTS AND DISCUSSION

Sequence analysis of BceAmiF. A BLAST search with the nucleotide sequence of the formamidase from *B. cereus* CECT 5050T (*BceamiF*) revealed 100% identity with the locus tags BC_3939 (annotated as an amidase gene) from *Bacillus cereus* ATCC 14579 (GenBank accession no. AE016877) and BCB4264_A4041 (annotated as a hydrolase gene of the carbon-nitrogen family) from *Bacillus cereus* B4264 (GenBank accession no. CP001176). Using the translated sequence of BceAmiF to carry out a BLAST search, the highest identity found with an enzyme of known activity was with the formamidase of *Helicobacter pylori* (HpyAmiF; GenBank accession no. O25836) (77% similarity). Sequence alignment of formamidases from several organisms classified under EC 3.5.1.49 with proven activity toward formamide, i.e., HpyAmiF (GenBank accession no. O25836), BceAmiF (this work), the *Methylophilus methylotrophus* enzyme (GenBank accession no. DAA01135), the *Paracoccidioides brasiliensis* enzyme (PbraFmdS; GenBank accession no. AAN87355), and the *Emericella nidulans* enzyme (GenBank accession no.

AAG60585), revealed sequence similarities of <10%, except for that with HpyAmiF. A BLAST search for similar available sequences, using BceAmiF and PbraFmdS as representatives, followed by multiple alignment and phylogenetic analysis, was carried out to study the classification of formamidases (Fig. 1). The first group was represented by derivatives of *H. pylori* AmiF and contained BceAmiF (AmiF clan). The second group (FmdS clan) was formed by members of the FmdA-AmdA family (PFAM protein family PF03069), and the similarity between the two groups was <10%. BceAmiF also presented sequence similarity to different amidases, such as aliphatic amidases, acylamide amidohydrolases, and nitrilase/cyanide hydratases (amidase clan). In this sense, it has already been proposed that aliphatic amidase and formamidase from *H. pylori* are paralogous enzymes that evolved after ancestral gene duplication (48). At the same time, Fig. 1 (see underlined sequences and nomenclature in the legend) reflects the large proportion of erroneously annotated proteins already shown by Engelhardt et al. (see reference 15 and references therein), derived from imprecise computational techniques or by deduction using another incorrect annotation.

3D modeling. The structural model of BceAmiF was determined using the known 1.75-Å-resolution crystal structure of HpyAmiF (PDB accession no. 2DYU) (23) and the Swiss-Model server (46). The quality of the models was assessed using the QMean and PROCHECK programs (4, 30, 31).

Overall averages for the QMean score (0.63) and G factor under accession numbers HQ542192 and ADQ27473.

(0.03) were recorded (QMean scores range between 0 and 1, with higher values for better models, and G factor scores should be above -0.5). Ramachandran plot statistics indicated that 86.2% of the main chain dihedral angles are found in the most favorable region and that 11.9% are located in additional allowed regions. Ideally, one would hope to have over 90% of the residues in these “core” regions. These results indicate that the homology model is reasonable. The final model included 313 residues of a total of 346. The omitted residues were at the N (12 residues) and C (21 residues) termini.

On the structural level, HpyAmiF has already been classified as a member of the nitrilase superfamily based on its X-ray

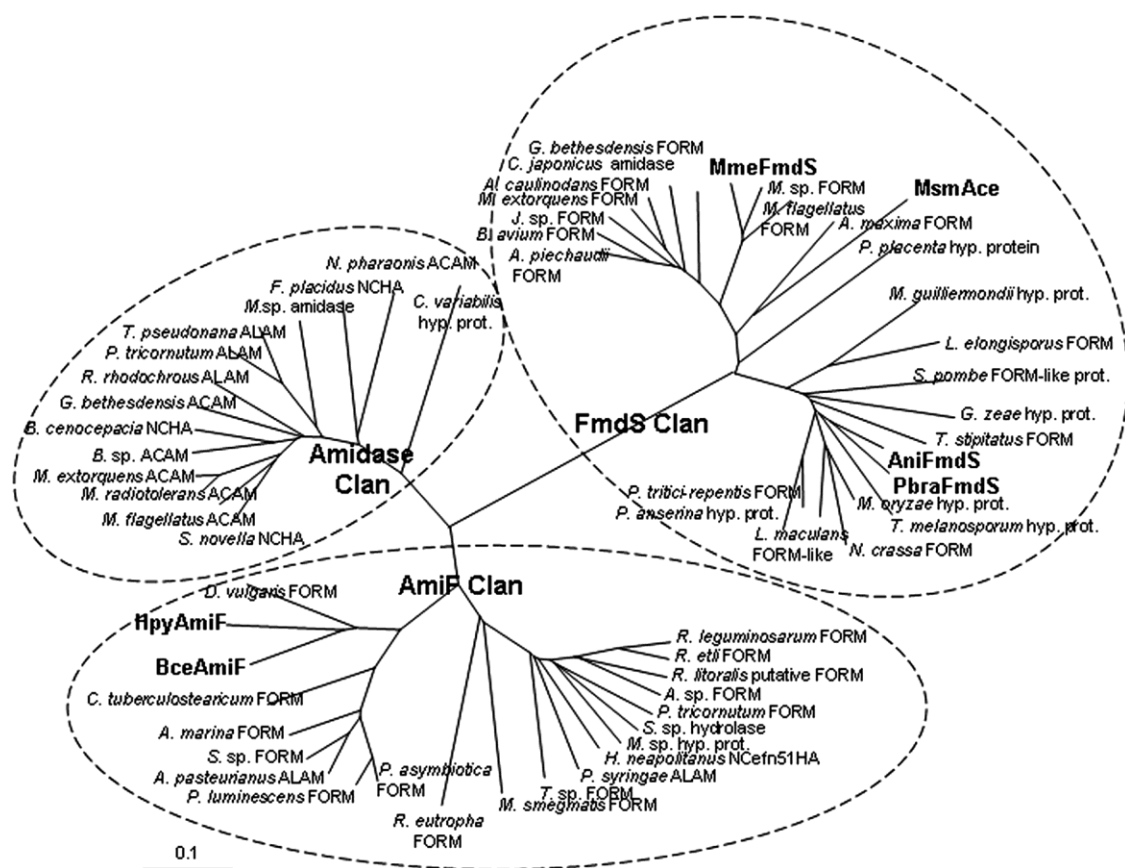


FIG. 1. Phylogenetic tree showing the relationships among formamidases with experimentally proven activity (bold) classified under EC 3.5.1.49 and among other amidases. The initial BLAST search was conducted with BceAmiF and PbraFmdS sequences. Clustal W XXL (28) was used for alignment, and the TREEVIEW (42) program was used to produce an unrooted phylogenetic tree. Sequences underlined in this legend are those whose database annotation might be misclassified. Abbreviations: FORM, formamidase; NCHA, nitrilase/cyanide hydratase and apolipoprotein N-acyltransferase; ALAM, alphatic amidase; ACAM, acylamide amidohydrolase; hyp. prot., hypothetical or predicted protein. Sequences under the following GenBank accession numbers were used for the AmiF clan: YP_770627, *Rhizobium leguminosarum* FORM; ZP_03518337, *Rhizobium etli* FORM; ZP_02141823, *Roseobacter litoralis* putative FORM; ZP_07373136.1, *Ahrensia* sp. FORM; XP_002179811, *Phaeodactylum tricorutum* FORM; ZP_05038498, *Synechococcus* sp. hydrolase of the carbon-nitrogen family; XP_002504646, *Micromonas* sp. predicted protein; YP_003263467, *Halothiobacillus neapolitanus* NCFn51HA; NP_791184, *Pseudomonas syringae* ALAM; CAZ90216, *Thiomonas* sp. FORM; YP_887708, *Mycobacterium smegmatis* FORM; YP_841971, *Ralstonia eutropha* FORM; YP_003041850, *Photobacterium asymbiotica* FORM; NP_930440, *Photobacterium luminescens* FORM; YP_003186690, *Acetobacter pasteurianus* ALAM; YP_382893, *Synechococcus* sp. FORM; YP_001521158, *Acaryochloris marina* FORM; ZP_05364864, *Corynebacterium tuberculostearicum* FORM; ADQ27473, *Bacillus cereus* FORM (BceAmiF); O25836, *Helicobacter pylori* FORM (HpyAmiF); and YP_010383, *Desulfovibrio vulgaris* FORM. Sequences under the following GenBank accession numbers were used for the amidase clan: YP_003695074, *Starkeya novella* NCHA; YP_544574, *Methylobacillus flagellatus* ACAM; YP_001758132, *Methylobacterium radiotolerans* ACAM; YP_001640829, *Methylobacterium extorquens* ACAM; YP_372600, *Burkholderia* sp. ACAM; ZP_04941504, *Burkholderia cenocepacia* NCHA; YP_745660, *Granulibacter bethesdensis* ACAM; AAX83004, *Rhodococcus rhodochrous* ALAM; XP_002183544, *Phaeodactylum tricorutum* ALAM; YP_002289996, *Thalassiosira pseudonana* ALAM; XP_002505633, *Micromonas* sp. amidase; YP_003434849, *Ferroglobus placidus* NCHA; YP_330835, *Natronomonas pharaonis* ACAM; and EFN51574, *Chlorella variabilis* hypothetical protein CHLNCDRAFT_140067. Sequences under the following GenBank accession numbers were used for the FmdS clan: ZP_06688672, *Achromobacter piechaudii* FORM; YP_786775, *Bordetella avium* FORM; YP_00135358, *Janthinobacterium* sp. FORM; YP_001640832, *Methylobacterium extorquens* FORM; YP_001527017, *Azorhizobium caulinodans* FORM; YP_001981459, *Cellvibrio japonicus* amidase; YP_745652, *Granulibacter bethesdensis* FORM; DAA01135, *Methylophilus methylotrophus* FORM (MmeFmdS); YP_004039140, *Methylovorus* sp. FORM; YP_545886, *Methylobacillus flagellatus* FORM; ZP_03273319, *Arthrospira maxima* FORM; DAA01135, *Mycobacterium smegmatis* acetamidase (MsmAce); XP_002474791, *Postia placenta* predicted protein; XP_001483206, *Meyerozyma guilliermondii* hypothetical protein PGUG_05161; XP_001526177, *Lodderomyces elongisporus* FORM; NP_595015, *Schizosaccharomyces pombe* FORM-like protein; XP_389218, *Gibberella zeae* hypothetical protein FG09042.1; XP_002487504, *Talaromyces stipitatus* FORM; AAG60585, *Emericella nidulans* FORM (AniFmdS); AAN87355, *Paracoccidioides brasiliensis* FORM (PbraFmdS); XP_360990, *Magnaporthe oryzae* hypothetical protein MGG_03533; XP_001932162, *Pyrenophora tritici-repentis* FORM (FmdS); XP_002835486, *Tuber melanosporum* hypothetical protein; XP_959782, *Neurospora crassa* FORM; XP_001929790, *Podospora anserina* hypothetical protein; and CBY02046, *Leptosphaeria maculans* FORM (similar).

structure (7, 23). Hung et al. (23) identified several homologs of AmiF by using the DALI server (22). Other homologs of the family identified in a new search are summarized in Table 1, with sequence identities with BceAmiF in the range of 17 to

35%. A catalytic C-E-K triad was discovered for the whole nitrilase superfamily (8, 40, 41). The modeled BceAmiF protein allowed us to identify three residues in the environment of the C-E-K triad which might be involved in enzyme activity:

TABLE 1. Several homologous enzymes of AmiF formamidase obtained using the DALI server (22), using the modeled BceAmiF enzyme as input^a

Enzyme	PDB ID	Reference	Z score	% Identity	C-E-E-K tetrad				Other residue(s) of interest
					Residue 1	Residue 2	Residue 3	Residue 4	
BceAmiF					E60	K132	E140	C165	W136, Y191
HpyAmiF	2DYUB	22	53.7	77	E60	K133	E141	C166	W137, Y192
Aliphatic amidase	2UXYA	2	40.1	33	E59	K134	E142	C166	W138, Y192
Aliphatic amidase	2PLQA	25	39.9	35	E59	K134	E142	C166	W138, Y192
Nitrilase homolog 2	2W1VA	3	33.4	23	E81	K150	E166	C191	F154, F217
Hypothetical protein PH0642	1J31D	41	32.1	26	E42	K113	E120	C146	F117, L172
32.5-kDa protein YLR351C	1F89A	26	31.8	26	E53	K128	E144	C169	A194/Y232
NIT (fragile histidine triad fusion protein)	1EMSB	38	31.8	21	E54	K127	E145	C169	F195
Nitrilase	3IVZA	40	31.7	25	E42	K113	E120	C146	F117, L172
γ-Alanine synthase	2VHIG	31	30.6	22	E120	K197	E208	C234	P201, T260
D-Carbamoylase	2GGLD	11	30.4	20	E47	K127	E146	C172	P131, T198
Putative Nit protein XC1258	2E11D	10	30.0	17	E43	K109	E118	C143	F113, W175
Amidase	3HKXA	NP	29.9	19	E61	K131	E139	C165	Y135, L191
Glutamine NAD ⁺ synthetase	3DLAC	28	28.8	21	E52	K121	E132	C176	P125, S203
NH ₃ -NAD ⁺ synthetase	3N05A	NP	26.1	18	E43	K125	E136	C161	P129, S188

^a Only structures with a Z value of >20 are presented. Residues are numbered as they appear in the PDB file. Structural alignment was carried out with Swiss-PDB Viewer. NP, not yet published.

Trp136, Glu140, and Tyr191 (see Fig. S1 in the supplemental material). Whereas Trp136 and Tyr191 are conserved only in formamidases and aliphatic amidases, structural alignment carried out on all of the structures revealed that Glu140 is positionally conserved in all of them (Table 1), which represent branches 2, 5, 6, 7, 8, and 10 of the nitrilase superfamily (8).

Expression, purification, and molecular mass analysis of wild-type BceAmiF and mutants. BceAmiF proteins with and without a His₆ tag were compared to analyze the effect of the His₆ tag on enzyme activity, and they showed no difference

(2.9 ± 0.3 and 2.8 ± 0.5 mmol formamide mg⁻¹ min⁻¹, respectively). It was therefore decided to continue all experiments with His₆-tagged BceAmiF. Its purification yielded 30 to 40 mg liter of culture⁻¹. SDS-PAGE analysis indicated that the wild-type BceAmiF enzyme was over 95% pure after elution from the affinity column (Fig. 2A), with an estimated molecular mass of 38 kDa (the deduced mass from the amino acid sequence, including the His₆ tag, is 38,632 Da). MALDI-TOF-TOF peptide mass fingerprinting analysis matched (score of 566) with the formamidase from *Bacillus cereus* ATCC 14579

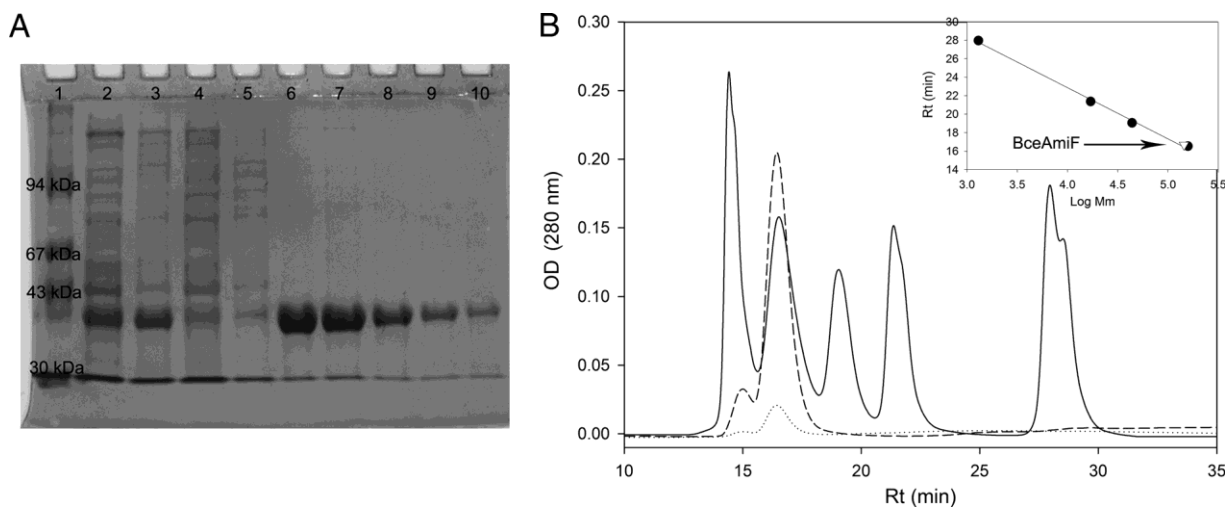


FIG. 2. (A) SDS-PAGE analysis of each step of purification of the formamidase from *Bacillus cereus* CECT 5050T. Lane 1, low-molecular-mass marker; lanes 2 and 3, supernatant and pellet of the resuspended crude extract after cell sonication; lane 4, eluate after adding the sonicated supernatant to the metal-affinity column; lane 5, flowthrough after washing the metal-affinity column with buffer; lanes 6 to 10, purified BceAmiF. (B) Size-exclusion chromatography of purified BceAmiF at 1 mg ml⁻¹ (dashed line) and 0.1 mg ml⁻¹ (dotted line) and of a gel filtration standard (Bio-Rad) (solid line). The inset represents the fit of retention times (Rt) versus the logarithms of the molecular masses of the protein markers (black circles). The arrow shows the Rt for BceAmiF (white triangle), showing a homotetrameric native structure.

(GenBank accession no. NP_833658), confirming the identity of BceAmiF. The other known member of the AmiF clan (HpyAmiF) presented a molecular mass of 34 kDa (48), whereas PbraFmdS and MmeFmdS of the FmdS clan presented masses of 45 and 44 kDa, respectively (5, 53, 54). The oligomeric structures of HpyAmiF, PbraFmdS, and MmeFmdS are described as hexameric, tetrameric, and trimeric, respectively (5, 23, 53). The relative molecular mass of the wild-type BceAmiF protein in the range of pH 5.5 to 9.0 was estimated to be 135 to 160 kDa by size-exclusion chromatography using a Superdex 200 HR column, suggesting that the native form of BceAmiF is a tetramer (Fig. 2B).

The purification of the W136H mutant was not successful, as this mutation caused the absence of overexpression of the enzyme (data not shown). The other mutants (E140D and Y191F) also presented purities of >95% (see Fig. S2 in the supplemental material) and similar relative molecular masses to that of wild-type BceAmiF at pH 6.0.

Effects of pH and temperature on activity. The formamidase enzyme showed maximum activity in citrate and cacodylate buffers at pH 6.0 when it was examined in 100 mM sodium citrate (pH 4.0 to 6.0), 100 mM sodium cacodylate (pH 6.0 to 7.5), 100 mM phosphate buffer (pH 6.0 to 8.0), and 100 mM borate-HCl or NaOH (pH 8.0 to 9.0) (Fig. 3A). The optimum temperature for hydrolysis of formamide was 50°C (Fig. 3B). The same optimum pH and a similar optimum temperature (45°C) were found for HpyAmiF (48). The thermal stability of BceAmiF was studied by means of two techniques: (i) preincubating the enzyme in 100 mM citrate buffer, pH 6.0, at different temperatures, and subsequently measuring the residual activity with the standard assay; and (ii) following the denaturation curve by means of far-UV CD. Activity was gradually lost when the enzyme was incubated at temperatures over 65°C for 30 min (Fig. 4). Furthermore, after incubation at the optimal temperature for activity of the enzyme (50°C) for 40 h, the enzyme maintained around 95% of its initial activity. Thermal denaturation of the enzyme followed by far-UV CD showed a melting temperature (T_m) for BceAmiF of $73.5 \pm 0.4^\circ\text{C}$ (Fig. 4), which is in agreement with the results obtained by measuring the residual activity after preincubation. In addition, these results confirm the high thermostability of this enzyme.

Effects of metals and chemical agents. Activity of the purified BceAmiF enzyme was assayed in the presence of a 2 mM concentration of different metal ions, 100 mM DTT and EDTA, and up to 50 mM iodoacetamide (Table 2). Activity was tested after 60 min of incubation with each reagent, using the standard assay. The presence of K^+ , Na^+ , Ca^{2+} , Mg^{2+} , Pb^{2+} , EDTA, and DTT had no significant effect on enzyme activity. Incubation with Hg^{2+} and with concentrations of iodoacetamide of >15 mM produced total inactivation of the BceAmiF enzyme. Similar results were observed with iodoacetate for HpyAmiF (48), and they are the result of the presence of a cysteine residue involved in catalysis.

Interestingly, using sodium phosphate as the buffering agent (as opposed to cacodylate/citrate), a decrease in enzyme activity was observed at the same pH (Fig. 3A). Inhibition of BceAmiF by phosphate anions was assayed with increasing concentrations of sodium phosphate, pH 6.0 (10 to 200 mM), in 100 mM sodium citrate, pH 6.0, with a decrease in activity of

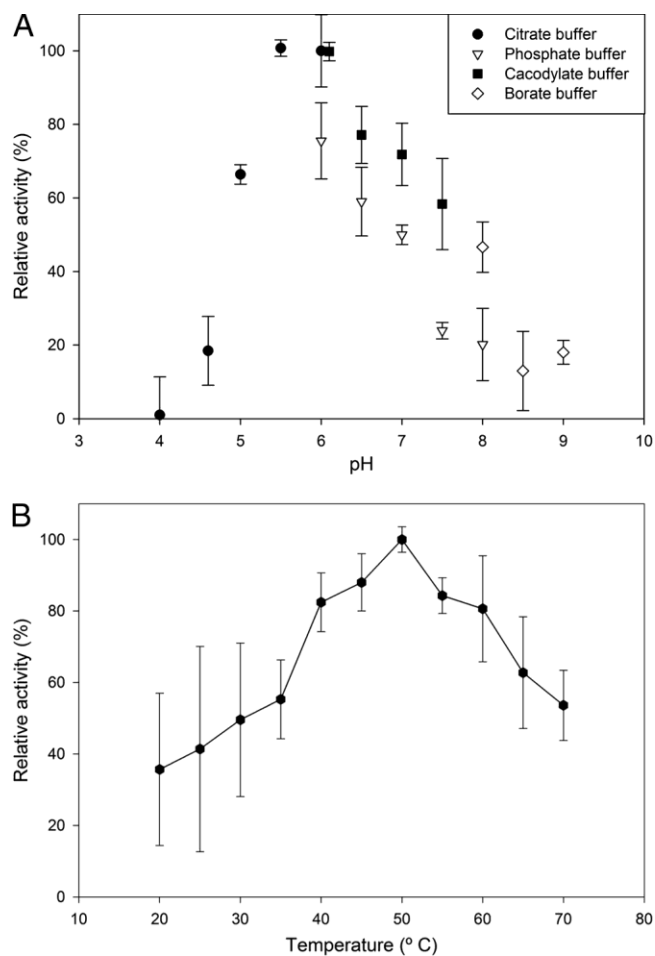


FIG. 3. Effects of pH (A) and temperature (B) on BceAmiF activity. The results are the means for three experiments, and the error bars indicate the standard deviations of the means.

up to 30%. Fluorescence binding experiments were conducted in order to determine whether phosphate anions could bind the enzyme (see Fig. S3A in the supplemental material), giving a binding constant (K) at 25°C of $2,811.7 \pm 338.9 \text{ M}^{-1}$, assuming four binding sites. Given the chemical similarity between phosphate anions and formamide and the results showing an arsenic adduct in the active site of the XC1258 enzyme from *Xanthomonas campestris* (11), we hypothesize that this molecule binds in the catalytic site.

Substrate specificity and kinetic assays. The substrate specificity of formamidases is poorly studied. Only one member of the FmdS clan, MmeFmdS, has been analyzed in this sense, proving able to hydrolyze formamide, propionamide, acetamide, butyramide, and acrylamide but not urea (54). The other studied member of the AmiF clan, HpyAmiF, does not hydrolyze urea, propionamide, acetamide, or acrylamide (48). Several amide substrates were tested with wild-type BceAmiF. Formamide was the best substrate by far, although the enzyme also recognized acetamide ($0.72 \pm 0.1 \mu\text{mol acetamide mg}^{-1} \text{ min}^{-1}$). Propionamide, butyramide, isobutyramide, alaninamide, leucinamide, glycinamide, and urea were not recognized as substrates. Acyltransferase activity is normally found

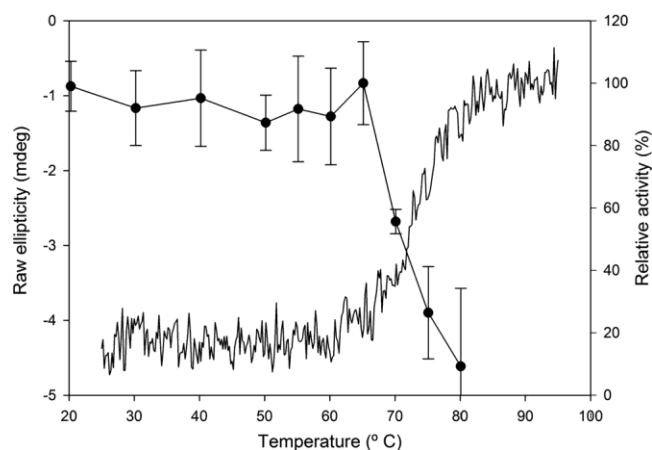


FIG. 4. CD-thermal denaturation analysis of BceAmiF, monitored by the changes in ellipticity at 222 nm (solid line; left axis) and the remaining relative activity of BceAmiF after a 30-min preincubation at the corresponding temperature (black circles; right axis). The results showing the remaining activity of BceAmiF are the means for three experiments, and the error bars indicate the standard deviations of the means.

in aliphatic amidases but was not detected for HpyAmiF (48). Formyl- and acetyltransferase activities were assayed using formamide, formate, acetamide, and acetate as donors and hydroxylamine as the acceptor. Both activities were detected, although the formate-hydroxamic compound formed during the reaction decomposed spontaneously, as described previously (16), and therefore the kinetic values could not be determined. The acyltransferase specific activity of BceAmiF using acetamide as a donor was $0.15 \pm 0.03 \mu\text{mol mg}^{-1} \text{min}^{-1}$. Transferase activity was not detected with propionamide, butyramide, or isobutyramide.

Although enzymes from the nitrilase superfamily are known to present a ping-pong mechanism (16), the kinetics of known formamidases have been calculated from hyperbolic saturation curves by least-square fitting of the data to the Michaelis-Menten equation (48), assuming that the second reaction (in which the formyl enzyme intermediate reacts with H_2O to produce the formiate product) is much faster than the previous one, which means that the first reaction governs the kinetics. Reactions were carried out with formamide at different concentrations (0.1 to 390 mM) at 50°C and pH 6.0, with a constant enzyme concentration of 52 nM. Under these conditions,

TABLE 2. Effects of different compounds on BceAmiF activity

Compound	Relative BceAmiF activity (%) ^a
Control	100 ± 7.1
Mg ²⁺	103.5 ± 9.0
Ca ²⁺	108.0 ± 8.1
K ⁺	101.9 ± 8.0
Na ⁺	97.0 ± 6.0
Pb ²⁺	104.1 ± 5.8
Hg ²⁺	0 ± 0
EDTA	106.0 ± 8.3
DTT	105.0 ± 4.9
Iodoacetamide	0 ± 0

^a Data are means ± standard deviations.

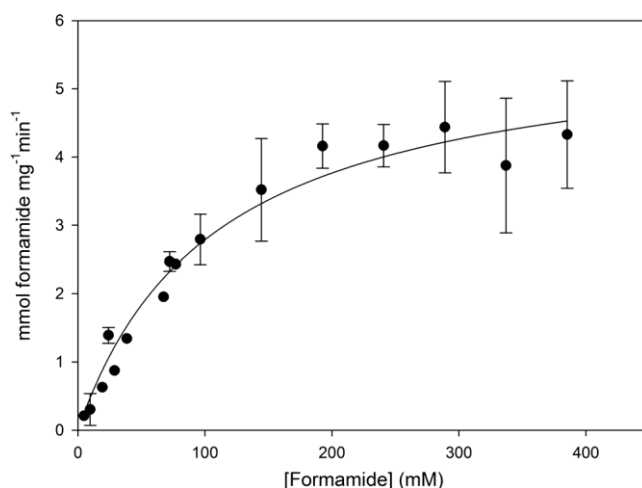


FIG. 5. Hyperbolic saturation curve of BceAmiF with formamide as a substrate. Apparent K_m and k_{cat} values were $108.0 \pm 16.9 \text{ mM}$ and $5.8 \pm 0.4 \text{ mmol mg}^{-1} \text{min}^{-1}$, respectively. The results are the means for three experiments, and the error bars indicate the standard deviations of the means.

the apparent K_m and k_{cat} values were $108.0 \pm 16.9 \text{ mM}$ and $5.8 \pm 0.4 \text{ mmol formiate min}^{-1} \text{mg}^{-1}$, respectively (Fig. 5). The K_m and k_{cat} values for HpyAmiF were $32.0 \pm 8.7 \text{ mM}$ and $1,081 \pm 114 \text{ mmol NH}_3 \text{ min}^{-1} \text{mg}^{-1}$, respectively (48), both on the same order of magnitude as those for BceAmiF, although slightly lower.

Effects of Glu140 and Tyr191 on the activity of the enzyme.

In order to evaluate the involvement of several residues identified in the modeled BceAmiF protein around the C-E-K triad (see Fig. S1 in the supplemental material), three mutants were created: the W136H, E140D, and Y191F mutants. The former could not be expressed or purified, suggesting that this residue has an essential role in the conformational stability of BceAmiF, as observed for Asp168 of HpyAmiF (48). Far-UV CD spectra were collected to evaluate the correct folding of the E140D and Y191F mutants. No significant differences were found in their secondary structure compared to the wild type (data not shown). Furthermore, thermal denaturations were followed by CD for the wild-type enzyme and the E140D and Y191F mutants. In all cases, the thermal denaturations were irreversible, and therefore it was not possible to estimate the thermodynamic parameters governing thermal unfolding. However, it was possible to determine the T_m , as described for other proteins showing irreversible thermal denaturations (19, 38). The obtained values were $73.2 \pm 1.2^\circ\text{C}$ for the E140D mutant and $72.5 \pm 0.4^\circ\text{C}$ for the Y191F mutant. On the other hand, the slight differences in T_m of the wild-type ($73.5 \pm 0.4^\circ\text{C}$) and mutated BceAmiF enzymes suggest that the mutations did not significantly alter BceAmiF folding, allowing us to hypothesize on the role of the two residues. The E140D mutant showed no detectable activity for up to 7 μM enzyme (135 times the standard concentration used for the wild-type enzyme), whereas the Y191F mutant showed activity of $11.8\% \pm 5.0\%$ compared to that of wild-type BceAmiF.

Fluorescence binding experiments were conducted in order to ascertain whether the E140D mutant could still bind formamide (see Fig. S3B in the supplemental material), giving a

binding constant (K) at 25°C of $683.5 \pm 41.1 \text{ M}^{-1}$. Furthermore, taking advantage of the inhibition of BceAmiF by phosphate, binding experiments with the E140D and Y191F mutants were carried out with this inhibitor to study their involvement in substrate binding, giving binding constants at 25°C of $1,953.3 \pm 352.7$ and $1,870.0 \pm 292.5 \text{ M}^{-1}$, respectively. Both are slightly lower than that obtained for the wild type but are on the same order of magnitude, indicating that the mutations did not significantly alter the catalytic environment. Thus, Tyr191 does not seem as critical for enzymatic activity as Glu140. The E140D mutant lacked any detectable activity but was still able to bind formamide, proving that it has a key role in hydrolysis of the substrate. In fact, in the seminal works of Brenner's group in which the C-E-K triad was discovered (8, 40, 41), the high conservation of this glutamic acid was already identified (see, for instance, Fig. 1 of reference 41), as was its position in the active site of NitFhit (PDB accession no. 1EMS). The HpyAmiF structure already suggested the involvement of the counterpart glutamate residue to maintain the side chain geometry of the catalytic C-E-K triad as well as to facilitate the docking of a substrate (23). Furthermore, the presence of that glutamate residue has also been pinpointed as necessary in homologous enzymes (2, 26, 44, 48a), but until this work, no experimental results were presented. Due to inconsistencies in the interpretation of Glu144 in the structure under PDB accession no. 1F89 (26), Kimani et al. only speculated on the role of Glu142 in aliphatic amidases (counterpart of BceAmiF Glu140; PDB accession no. 2PLQ) (Table 1) as a general second base.

We carried out further studies using the Conserved Domain Database (CDD), which has reclassified the nitrilase superfamily, including nitrile- or amide-hydrolyzing enzymes and amide-condensing enzymes (36). This hierarchy (CL11424) includes the different enzyme classes described previously (8), as well as new additional subfamilies (subfamilies cd07564 to cd07587). This new classification shows some mismatches of the consistently identified C-E-K triad (exceptions have been found for subfamilies cd07566, cd07567, cd07573, cd07579, cd07582, and cd07585 [Table 1; see Fig. S4 in the supplemental material]). The presence of the conserved glutamic acid (Table 1) discussed above also presents exceptions (subfamilies cd07566, cd07573, cd07576, cd07579, cd07582, and cd07585). To conclude, full conservation of the C-E-E-K tetrad is found in 17 of 24 subfamilies. Bearing these data in mind, what was hitherto considered the C-E-K triad is in fact a C-E-E-K catalytic tetrad for several members of the nitrilase superfamily (Fig. 6). Based on the results presented in this work, we can conclude that this glutamic acid residue (Glu140 in BceAmiF) is involved in substrate hydrolysis, but we do not know whether it acts (i) as a second general base catalyst which allows hydrolysis of the acyl intermediate of the substrate, as proposed by Kimani et al. (26); or (ii) as a polarizer/costabilizer of the catalytic lysine of the intermediate of the reaction, allowing the stabilization of a tetrahedral intermediate of the reaction (2, 23). On the other hand, for the specific case of formamidases and aliphatic amidases (Table 1), Tyr191 is at hydrogen bond distance from Glu140 (2.3 Å in the formamidase structure under PDB accession no. 2DYU) and may alter the charge distribution of the lateral chain of Glu140 to assist in its function. The absence of the hydroxyl group in the Y191F mutant might decrease (but

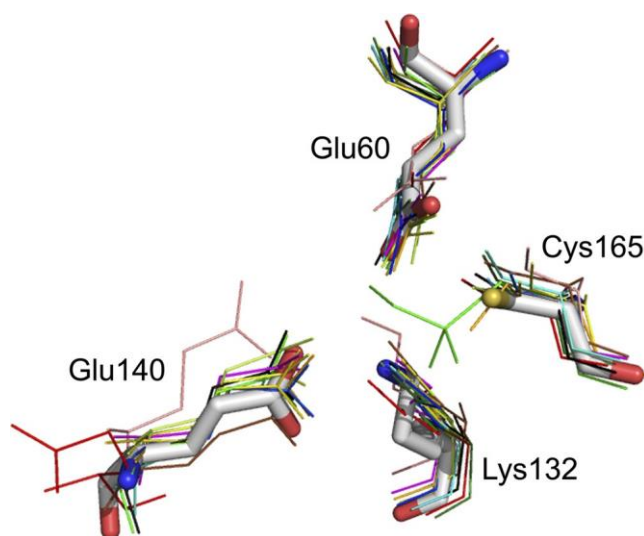


FIG. 6. Superposition of the conserved C-E-E-K tetrads of several members of the nitrilase superfamily. Positional conservation was previously highlighted by Thuku et al. (48a). The BceAmiF model (sticks; CPK) is shown, along with the following structures (PDB accession no.): formamidase (2DYU; blue [23]), aliphatic amidases (2UXY [green, showing an acyl intermediate (2)] and 2PLQ [black]), nitrilase homolog 2 (2W1V; dark green [3]), hypothetical protein PH0642 (1J31; dark blue [45]), YLR351C (1F89; red [27]), NIT (fragile histidine nitrilase triad fusion protein) (1EMS; brown [41]), β -alanine synthase (2VHI; lemon [33]), D-carbamoylase (2GGL; magenta [12]), hydrolase (2E11; sky blue [11]), amidase (3HKX; yellow-orange [39a]), glutamine NAD^+ synthetase (3DLA; yellow [29]), and NH_3 - NAD^+ synthetase (3N05; salmon).

not completely eliminate) the electrophilic character of the carboxyl moiety of Glu140, resulting in a lower activity of the enzyme.

ACKNOWLEDGMENTS

This work was supported by the Spanish Ministry of Education and Science, the European Social Fund (ESF), and the European Regional Development Fund (ERDF), through projects BIO2007-67009, SAF2008-05742-C02-01, CSD2008-000005, and AIMG grant BES-2008-003751; by the Andalusian Regional Council of Innovation, Science and Technology, through projects CV7-02651 and TEP-4691; by the Generalitat Valenciana, through project ACOMP/2011/113; and by the European Science Foundation COST, through action CM0701. P.S.-M. was supported by the University of Almería. S.M.-R. was supported by the Andalusian Regional Government.

We thank Andy Taylor for critical discussion of the manuscript and Pedro Madrid-Romero for technical assistance.

REFERENCES

- Altschul, S. F., W. Gish, W. Miller, E. W. Myers, and D. J. Lipman. 1990. Basic local alignment search tool. *J. Mol. Biol.* **215**:403–410.
- Andrade, J., A. Karmali, M. A. Carrondo, and C. Frazaõ. 2007. Structure of amidase from *Pseudomonas aeruginosa* showing a trapped acyl transfer reaction intermediate state. *J. Biol. Chem.* **282**:19598–19605.
- Barglow, K. T., et al. 2008. Functional proteomic and structural insights into molecular recognition in the nitrilase family enzymes. *Biochemistry* **47**:13514–13523.
- Benkert, P., M. Kuñzli, and T. Schwede. 2009. QMEAN server for protein model quality estimation. *Nucleic Acids Res.* **37**:W510–W514.
- Borges, C. L., et al. 2010. Detection of a homotetrameric structure and protein-protein interactions of *Paracoccidioides brasiliensis* formamidase lead to new functional insights. *FEMS Yeast Res.* **10**:104–113.
- Borges, C. L., et al. 2005. The antigenic and catalytically active formamidase of *Paracoccidioides brasiliensis*: protein characterization, cDNA and gene cloning, heterologous expression and functional analysis of the recombinant protein. *Microbes Infect.* **7**:66–77.

7. Bork, P., and E. V. Koonin. 1994. A new family of carbon-nitrogen hydrolases. *Protein Sci.* **3**:1344–1346.
8. Brenner, C. 2002. Catalysis in the nitrilase superfamily. *Curr. Opin. Struct. Biol.* **12**:775–782.
9. Bury-Mon'è, S., et al. 2003. Presence of active aliphatic amidases in *Helicobacter* species able to colonize the stomach. *Infect. Immun.* **71**:5613–5622.
10. Bury-Mon'è, S., et al. 2004. Responsiveness to acidity via metal ion regulators mediates virulence in the gastric pathogen *Helicobacter pylori*. *Mol. Microbiol.* **53**:623–638.
11. Chin, K. H., et al. 2007. The crystal structure of XC1258 from *Xanthomonas campestris*: a putative procaryotic Nit protein with an arsenic adduct in the active site. *Proteins* **69**:665–671.
12. Chiu, W. C., et al. 2006. Structure-stability-activity relationship in covalently cross-linked *N*-carbamoyl *D*-amino acid amidohydrolase and *N*-acylamino acid racemase. *J. Mol. Biol.* **359**:741–753.
13. Draper, P. 1967. The aliphatic acylamide amidohydrolase of *Mycobacterium smegmatis*: its inducible nature and relation to acyl-transfer to hydroxylamine. *J. Gen. Microbiol.* **46**:111–123.
14. Egorova, K., H. Trauthwein, S. Verseck, and G. Antranikian. 2004. Purification and properties of an enantioselective and thermoactive amidase from the thermophilic actinomycete *Pseudonocardia thermophila*. *Appl. Microbiol. Biotechnol.* **65**:38–45.
15. Engelhardt, B. E., M. I. Jordan, S. T. Repo, and S. E. Brenner. 2009. Phylogenetic molecular function annotation. *J. Phys.* **180**:12024.
16. Fournand, D., F. Bigey, and A. Arnaud. 1998. Acyl transfer activity of an amidase from *Rhodococcus* sp. strain R312: formation of a wide range of hydroxamic acids. *Appl. Environ. Microbiol.* **64**:2844–2852.
17. Fraser, J. A., M. A. Davis, and M. J. Hynes. 2001. The formamidase gene of *Aspergillus nidulans*: regulation by nitrogen metabolite repression and transcriptional interference by an overlapping upstream gene. *Genetics* **157**:119–131.
18. Friedrich, C. G., and G. Mitrenga. 1981. Utilization of aliphatic amides and formation of two different amidases by *Alcaligenes eutrophus*. *J. Gen. Microbiol.* **125**:367–374.
19. Galisteo, M. L., P. L. Mateo, and J. M. Sa'ñchez-Ruiz. 1991. Kinetic study on the irreversible thermal denaturation of yeast phosphoglycerate kinase. *Biochemistry* **30**:2061–2066.
20. Gill, S. C., and P. H. Von Hippel. 1989. Calculation of protein extinction coefficients from amino acid sequence data. *Anal. Biochem.* **182**:319–326.
21. Guex, N., and M. C. Peitsch. 1997. SWISS-MODEL and the Swiss-PdbViewer: an environment for comparative protein modeling. *Electrophoresis* **18**:2714–2723.
22. Holm, L., and P. Rosenström. 2010. Dali server: conservation mapping in 3D. *Nucleic Acids Res.* **38**:W545–W549.
23. Hung, C. L., et al. 2007. Crystal structure of *Helicobacter pylori* formamidase AmiF reveals a cysteine-glutamate-lysine catalytic triad. *J. Biol. Chem.* **282**:12220–12229.
24. Hynes, M. J. 1975. Amide utilization in *Aspergillus nidulans*: evidence for a third amidase enzyme. *J. Gen. Microbiol.* **91**:99–109.
25. Kaplan, W., and T. G. Littlejohn. 2001. Swiss-PDB Viewer (Deep View). *Brief. Bioinform.* **2**:195–197.
26. Kimani, S. W., V. B. Agarkar, D. A. Cowan, M. F. Sayed, and B. T. Sewell. 2007. Structure of an aliphatic amidase from *Geobacillus pallidus* RAPc8. *Acta Crystallogr. D Biol. Crystallogr.* **63**:1048–1058.
27. Kumaran, D., et al. 2003. Crystal structure of a putative CN hydrolase from yeast. *Proteins* **52**:283–291.
28. Larkin, M. A., et al. 2007. Clustal W and Clustal X version 2.0. *Bioinformatics* **23**:2947–2948.
29. LaRonde-LeBlanc, N., M. Resto, and B. Gerratana. 2009. Regulation of active site coupling in glutamine-dependent NAD(+) synthetase. *Nat. Struct. Mol. Biol.* **16**:421–429.
30. Laskowski, R. A., et al. 1997. PDBsum: a Web-based database of summaries and analyses of all PDB structures. *Trends Biochem. Sci.* **22**:488–490.
31. Laskowski, R. A., M. W. MacArthur, D. S. Moss, and J. M. Thornton. 1993. PROCHECK: a program to check the stereochemical quality of protein structures. *J. Appl. Crystallogr.* **26**:283–291.
32. Loh, J. T., and T. L. Cover. 2006. Requirement of histidine kinases HP0165 and HP1364 for acid resistance in *Helicobacter pylori*. *Infect. Immun.* **74**:3052–3059.
33. Lundgren, S., B. Lohkamp, B. Andersen, J. Pi'skur, and D. Dobritzsch. 2008. The crystal structure of β 3-alanine synthase from *Drosophila melanogaster* reveals a homooctameric helical turn-like assembly. *J. Mol. Biol.* **377**:1544–1559.
34. Mahenthiralingam, E., P. Draper, E. O. Davis, and M. J. Colston. 1993. Cloning and sequencing of the gene which encodes the highly inducible acetamidase of *Mycobacterium smegmatis*. *J. Gen. Microbiol.* **139**:575–583.
35. Makhongela, H. S., et al. 2007. A novel thermostable nitrilase superfamily amidase from *Geobacillus pallidus* showing acyl transfer activity. *Appl. Microbiol. Biotechnol.* **75**:801–811.
36. Marchler-Bauer, A., et al. 2011. CDD: a conserved domain database for the functional annotation of proteins. *Nucleic Acids Res.* **39**:D225–D229.
37. Martínez-Rodríguez, S., et al. 2006. Crystallization and preliminary crystallographic studies of the recombinant dihydropyrimidinase from *Sinorhizobium meliloti* CECT4114. *Acta Crystallogr. Sect. F Struct. Biol. Crystallogr. Commun.* **62**:1223–1226.
38. Martínez-Rodríguez, S., et al. 2009. Metal-triggered changes in the stability and secondary structure of a tetrameric dihydropyrimidinase: a biophysical characterization. *Biophys. Chem.* **139**:42–52.
39. Merrell, D. S., M. L. Goodrich, G. Otto, L. S. Tompkins, and S. Falkow. 2003. pH-regulated gene expression of the gastric pathogen *Helicobacter pylori*. *Infect. Immun.* **71**:3529–3539.
- 39a. Nel, A. J., I. M. Tuffin, B. T. Sewell, and D. A. Cowan. 2011. Unique aliphatic amidase from a psychrotrophic and haloalkaliphilic *Nesterenkonia* isolate. *Appl. Environ. Microbiol.* **77**:3696–3702.
40. Pace, H. C., and C. Brenner. 2001. The nitrilase superfamily: classification, structure and function. *Genome Biol.* **2**:reviews0001.1–reviews0001.9.
41. Pace, H. C., et al. 2000. Crystal structure of the worm NitFhit Rosetta Stone protein reveals a Nit tetramer binding two Fhit dimers. *Curr. Biol.* **10**:907–917.
42. Page, R. D. 1996. TreeView: an application to display phylogenetic trees on personal computers. *Comput. Appl. Biosci.* **12**:357–358.
43. Pflöck, M., et al. 2006. Characterization of the ArsRS regulon of *Helicobacter pylori*, involved in acid adaptation. *J. Bacteriol.* **188**:3449–3462.
44. Raczynska, J. E., C. E. Vorgias, G. Antranikian, and W. Rypniewski. 2011. Crystallographic analysis of a thermoactive nitrilase. *J. Struct. Biol.* **173**:294–302.
45. Sakai, N., Y. Tajika, M. Yao, N. Watanabe, and I. Tanaka. 2004. Crystal structure of hypothetical protein PH0642 from *Pyrococcus horikoshii* at 1.6 Å resolution. *Proteins* **57**:869–873.
46. Schwede, T., J. Kopp, N. Guex, and M. C. Peitsch. 2003. SWISS-MODEL: an automated protein homology-modeling server. *Nucleic Acids Res.* **31**:3381–3385.
47. Skouloubris, S., A. Labigne, and H. De Reuse. 1997. Identification and characterization of an aliphatic amidase in *Helicobacter pylori*. *Mol. Microbiol.* **25**:989–998.
48. Skouloubris, S., A. Labigne, and H. De Reuse. 2001. The AmiE aliphatic amidase and AmiF formamidase of *Helicobacter pylori*: natural evolution of two enzyme paralogues. *Mol. Microbiol.* **40**:596–609.
- 48a. Thuku, R. N., D. Brady, M. J. Benedik, and B. T. Sewell. 2009. Microbial nitrilases: versatile, spiral forming, industrial enzymes. *J. Appl. Microbiol.* **106**:703–727.
49. van Eys, G. J. J. M., et al. 1989. Detection of leptospires in urine PCR. *J. Clin. Microbiol.* **27**:2258–2262.
50. van Vliet, A. H. M., E. J. Kuipers, J. Stoof, S. W. Poppelaars, and J. G. Kusters. 2004. Acid-responsive gene induction of ammonia-producing enzymes in *Helicobacter pylori* is mediated via a metal-responsive repressor cascade. *Infect. Immun.* **72**:766–773.
51. van Vliet, A. H. M., et al. 2003. Differential regulation of amidase- and formamidase-mediated ammonia production by the *Helicobacter pylori* fur repressor. *J. Biol. Chem.* **278**:9052–9057.
52. Wen, Y., et al. 2003. Acid-adaptive genes of *Helicobacter pylori*. *Infect. Immun.* **71**:5921–5939.
53. Wyborn, N. R. 1996. Molecular characterisation of formamidase from *Methylophilus methylotrophus*. *Eur. J. Biochem.* **240**:314–322.
54. Wyborn, N. R., D. J. Scherr, and C. W. Jones. 1994. Purification, properties and heterologous expression of formamidase from *Methylophilus methylotrophus*. *Microbiology* **140**:191–195.